Phase-shifting real-time holographic interferometry that uses bismuth silicon oxide crystals

M. P. Georges and Ph. C. Lemaire

A bismuth silicon oxide crystal is used in the diffusion regime as a dynamic recording medium in a real-time holographic interferometer based on anisotropic self-diffraction. This device is connected with an interferogram-analysis method that uses the phase-shifting technique for quantitative measurement of diffusive-reflecting object deformations. In addition to the usual error sources in phase shifting, the temporal interferogram erasure is studied and is found weakly perturbative for the measured phase. It is shown that quantitative measurements are possible for low-intensity object beams (8 $\mu W/cm^2$) and a large observed area. A practical situation of defect monitoring in a composite structure is presented.

Key words: Holographic materials, holography, holography applications, interferometry, metrology, nondestructive testing, photorefractive materials.

1. Introduction

It is well established now that holographic interferometry (HI) is one of the most powerful methods for measuring displacement or deformation or detecting defects in numerous industrial problems.[1–3] For coping with industrial requirements, a holographic interferometer should be easy to use, rapidly reusable, and as fast as possible in giving results of quantitative measurement. The holographic recording material must then comply with these requirements. The ideal material should be self-developing *in situ*, reusable, highly sensitive, and capable of giving the largest diffraction efficiency. Currently, no recording medium has all these qualities, but some materials have most of them.

The silver halide emulsions[4] have a high sensitivity (density of recording energy from 0.5 to 50 $\mu J/cm^2$) but are not self-developing (they need chemical processing) and are not reusable. Photopolymers of different types[4] are self-developing, and, despite high diffraction efficiencies, they are weakly sensitive (of the order of 10 mJ/cm^2). Thermoplastic materials[4] are preferred because they are self-developing with a recording energy of $\sim$1 $\mu J/cm^2$. Although thermoplastic plates could be reused, this cannot be achieved with optimal performances, and thermoplastic films for one exposure are used.

Attractive alternative media for hologram recording in HI are the photorefractive crystals[5–7] (PRC's). These materials are photoabsorbing and electro-optic.[8] The electrons that are trapped in impurities can be photoexcited into the conduction band in the areas in which the crystal is illuminated. These electrons migrate toward the dark areas, in which they are trapped again. A space-charge field is then created between illuminated and nonilluminated zones that modulates the refractive index through the linear electro-optic effect. Photorefractive materials can then be used to store phase holograms through refractive-index modulation. They are then self-developing and indefinitely reusable because the hologram can be erased by homogeneous illumination that redistributes the electrons across the crystal. Their sensitivity varies as a function of the species and the experimental parameters, such as the wavelength, the charge-transport processes involved, and the writing angles.

The sillenite family [$Bi_{12}SiO_{20}$ (BSO), $Bi_{12}GeO_{20}$ (BGO), and $Bi_{12}TiO_{20}$ (BTO)] is among the most sensitive photorefractive crystals, with a recording energy of $\sim$1 mJ/cm^2. In these crystals the charge migration can take place under thermal diffusion, referred to as the diffusion regime, and under an applied bias electric field, it is referred to as the drift regime. The drift regime leads to higher diffraction

The authors are with the Centre Spatial de Liège, Université de Liège, Parc Scientifique du Sart Tilman, Avenue du Pré-Aily, Liege 4031, Belgium.

Received 4 April 1995.
0003-6935/95/327497-10$06.00/0.

efficiencies than in diffusion, but in the latter case, some polarization properties are helpful in the development of an optimized holographic interferometer.

Although various authors have shown qualitative measurements with HI using sillenites,[5–7,9,10] there have been few attempts to connect such systems with an automated fringe-analysis system that leads to quantitative results. Vlad *et al.*[11] have used an intensity-based analysis method applied to various measurements on transparent objects with a BTO interferometer. Dirksen and von Bally[12] have recently reported measurements of deformation of a diffusive-reflecting object obtained by a double-exposure BTO interferometer and a Fourier-transform (FT) -based analysis method. Tiziani[13] has shown measurements of curing glue obtained by an interferometer with BSO in the drift regime and a phase-shifting analysis method.

In this paper we show that it is possible to use a BSO crystal in the diffusion regime in a real-time interferometer that uses a phase-shifting processing of interferograms. The configuration used is based on anisotropic self-diffraction, already presented by various authors[10,14]; it has the double advantage of working at the same wavelength in both writing and reading processes and of exhibiting a polarization separation between both interfering object fields. For the first time, to our knowledge, it is shown that it is possible to achieve quantitative measurement of deformations of diffusively reflecting objects with a weak object-beam intensity (of the order of 10 $\mu W/cm^2$) without special light-collecting systems, as used by others. Also, the characteristic time of the dynamic process is found to be compatible with the temporal phase-shifting process for quantitative evaluation. At last, the holographic head, which contains the crystal and polarizers and no bias field supply, can be set in front of a camera with an imaging objective. This setup leads to a holographic camera that is very compact compared with traditional thermoplastic cameras, which include clumsy thermal and electrical processing devices.

In Section 2, we recall the basic principles of anisotropic self-diffraction and its use for the production of interferograms in real-time holographic interferometry. Also, we briefly introduce the existing interferogram-analysis methods and explain the choice of phase shifting. We then discuss the trade-off that led us to the choice of the appropriate phase-shifting algorithm. In Section 3, we describe the experimentation of the phase shifting in photorefractive HI. The setup is presented, and some highlights concerning its optimization are discussed in reference to the literature. An analysis of the error on the quantitative phase measurement is done, which points out the decrease of interferogram modulation with time that is caused by dynamic crystal behavior. This effect is found to be nonperturbative in the optimal working conditions used in our setup for white diffusive objects. We then show results of a certification experiment of the method that consists of measuring the deformation of an aluminum plate. In Section 4 we present results of defect measurement in a composite structure.

2. Theoretical Background

A. Anisotropic Self-Diffraction in Real-Time Holographic Interferometry

Because PRC's generally have thicknesses of several millimeters, they can record thick phase holograms by local variations of the refractive index. In the case of extended objects the readout of the hologram must satisfy the Bragg conditions, and therefore the recording and the readout processes must be carried out at the same angle of incidence and wavelength. Kamshilin and Petrov[14] have shown the possibility of simultaneous recording and reading by using a two-wave technique: the readout beam is the same as the recording beam. A hologram is recorded in the crystal and corresponds to the first state of the object under consideration. Just after the object changes, interference fringes appear that correspond to the phase difference between both objects states. A new hologram corresponding to the second object state is then recorded and irreversibly replaces the first hologram; then the interferogram's contrast decreases at the same time. A major feature of this technique is the difference of polarization directions between the incident and the diffracted beams, coming from anisotropic self-diffraction. The optical activity, which acts at the same time as the electro-optic effect in sillenite crystals, also influences the polarization state of the light emerging from the crystal and the diffraction efficiency. According to Kogelnik's theory[15] on diffraction by thick gratings, the diffraction efficiency in the case of thick phase holograms with absorption is given by

$$\eta_0 = \exp(-\alpha l/\cos\theta)\sin^2\left(\frac{\pi \Delta n l}{\lambda \cos\theta}\right), \qquad (1)$$

where α is the absorption, l is the thickness, θ is the half-angle between reference and the object beams, Δn is the refractive-index variation, and λ is the wavelength. This expression does not take into account the effect of optical activity, which is necessary to calculate η. For doing this, the crystallographic configuration of the sample has to be considered. The crystals are generally cut such that the faces are normal to the crystallographic axes $\langle 110\rangle$, $\langle -110\rangle$, and $\langle 001\rangle$. Let us call $\mathbf{K}$ (Fig. 1) the wave vector that corresponds to the grating recorded inside the crystal ($\mathbf{K}$ has a direction perpendicular to the recorded fringes and a modulus equal to $2\pi/\Lambda$, with Λ the distance between two fringes). When $\mathbf{K}$ is parallel to $\langle 110\rangle$, the principal axes of induced birefringence x and y are rotated by 45° with respect to $\langle 001\rangle$ and $\langle 110\rangle$; the diffraction efficiency is optimum and does not depend on the orientation of readout polarization.[16,17]

In the particular case of the diffusion regime considered here, the expression of the diffraction

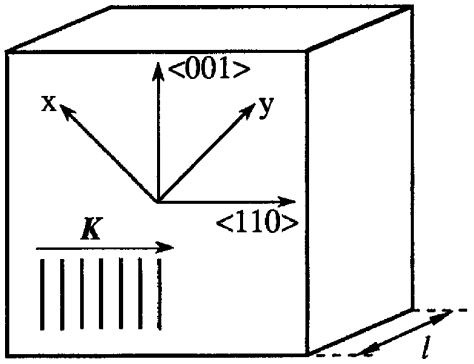

Fig. 1. BSO crystal configuration used for real-time holographic interferometry, with grating vector **K** parallel to the ⟨110⟩ direction.

efficiency can be approximated to the following expression:

$$\eta = \eta_0 \,\mathrm{sinc}^2(\rho l), \tag{2}$$

where ρ is the optical activity by unit length. This expression shows that there is an optimal thickness l that is dependent on crystal and experimental parameters; for classical values of these parameters the optimal thickness is from 2 to 3 mm for $\lambda = 514$ nm.

It is also shown[16] that the emerging diffracted polarization is linear and its orientation γ_d with respect to x is equal to $-\gamma_i$, where γ_i is the angle between the direction of the incident object-beam polarization and the principal axis x, i.e., the crystal acts as a half-wave plate on the diffracted beam (Fig. 2). This fact is of major importance in practice because the input polarization $\mathbf{P}_i$ can be orientated such that the transmitted linear polarization $\mathbf{P}_t$ emerges at right angles with respect to the diffracted linear polarization $\mathbf{P}_d$, as shown in Fig. 2. The solution is to orientate the input polarization at half the total polarization rotation angle ρl from the bisector axis of x and y, i.e., ⟨001⟩. Therefore a polarizer set at the crystal output can easily balance both transmitted and diffracted intensities in order obtain the maximum contrast in the interferogram.

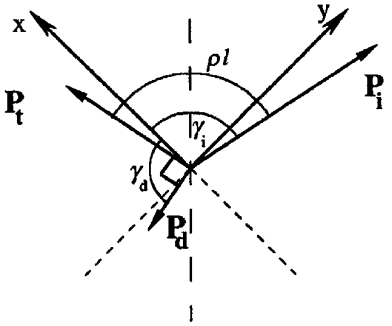

Fig. 2. Orientations of the linear polarizations of the different object beams involved with respect to the principal axis x of the crystal. Vectors $\mathbf{P}_i$, $\mathbf{P}_d$, and $\mathbf{P}_t$ are drawn with different lengths that are qualitatively proportional to the intensities of the corresponding beams.

B. Interferogram-Analysis Methods

In holographic interferometry the superposition of the waves, corresponding to the two states of the object under test, leads to an intensity pattern that varies as a function of the phase difference between both interfering fields. The interferogram has an intensity profile $I(u, v)$ given at each point (u, v) of an observation plane by

$$I(u, v) = I_0(u, v)\{1 + m(u, v)\cos[\phi(u, v)]\}, \tag{3}$$

where $I_0(u, v)$ is the average intensity of the pattern, $m(u, v)$ is the modulation of the interference, and $\phi(u, v)$ is the phase difference between diffracted and transmitted wave fronts. In order to obtain the quantitative difference in terms of displacement or deformation of the object, one has to determine the quantity $\phi(u, v)$ from the intensity pattern [Eq. (3)].

There exist different phase-evaluation methods.[2,18,19] A first class covers the intensity-based methods that are the modern extension of the former manual fringe counting. They consist of building the architecture of the fringes (by fringe tracking or skeletonizing); the result is a pattern of lines corresponding to the same phase value that remains to be interpolated to reconstruct the phase map. A second class is the spatial-carrier methods, among which the FT processing of the interferogram is extensively used. A last reknown class is the phase-shifting methods, which require acquisition of several interferograms shifted in phase with respect to each other.

Intensity-based methods have the advantage of requiring only one interferogram and of being easily implemented on computer, but they have the drawback that they generally require interaction with the operator and that the results have a low precision, generally λ to $\lambda/10$.[19] FT methods require only one interferogram; the measurement precision is at maximum $\lambda/30$,[19] but generally they suffer from complex processing.[18] Phase-shifting methods are simpler than the preceding in terms of computing effort for a measurement precision that can reach $\lambda/100$.[19] These considerations led us to choose the phase-shifting processing to be used in our holographic interferometer.

The phase-shifting technique requires the acquisition of several interferograms (at least three) that differ between each other by different amounts of phase introduced in the cosine of Eq. (3). Generally, one expresses the kth interferogram acquired in the phase-shifting sequence by

$$I_k(u, v) = I_0(u, v)\{1 + m(u, v)\cos[\phi(u, v) + \Delta\phi_k(u, v)]\}, \tag{4}$$

where $\Delta\phi_k(u, v)$ is the kth phase shift. There is a large number of phase-shifting algorithms.[18,19] A first class of algorithms requires calibrated shifts of phase between the interferograms before calculating $\phi(u, v)$. In these cases, $\Delta\phi_k(u, v)$ is supposed to be identical for all points (u, v) and also at each step, i.e.,

$\Delta\phi_k(u, v) = \Delta\phi$. A classical example is the four-frame algorithm with $\Delta\phi$ taking the successive values 0, $\pi/2$, π, and $3\pi/2$ and for which the phase $\phi(u, v)$ is calculated simply by

$$\phi(u, v) = \tan^{-1}\left(\frac{I_4 - I_2}{I_1 - I_3}\right). \tag{5}$$

For other algorithms of this class, different numbers and values of shifts are used in order to obtain a simple expression of the same type as Eq. (5).

Another type of algorithm, referred to as the general phase shift or the Carré algorithm, uses four frames with uncalibrated but equal shifts. In this case the phase is more complicated to calculate, and its expression is given by

$$\phi(u, v) = \tan^{-1}\left(\frac{\{(I_1 - I_4 + I_2 - I_3)[3(I_2 - I_3) - (I_1 - I_4)]\}^{1/2}}{(I_2 + I_3) - (I_1 + I_4)}\right). \tag{6}$$

The major sources of error present in the phase-shifting algorithms are the miscalibration and the nonlinearity of the phase-shifter device, the nonlinearity of the detection device (a CCD followed by a frame grabber), the quantization of the interferograms, and the vibration and air turbulences between acquisitions. These errors have been studied by various authors; a summary of these works can be found in different recent books.[2,18] In the particular case of real-time holographic interferometry in PRC's that use phase shifting of interferograms, another error source appears: the decrease of interferogram modulation $m(u, v)$ with respect to the time. This is extensively studied in Subsection 3.C.

We now briefly explain the choice of the phase-shifting algorithm. In regard to the phase-shifter miscalibration, the Carré algorithm is trivially insensitive and the algorithms with calibrated phase shift are sensitive to it, the less sensitive being the five-frame algorithm with $\pi/2$ shifts. In regard to quadratic nonlinearity of the phase shifter, the five-frame and the Carré algorithms are less sensitive than the four- and the three-frame algorithms. In regard to the nonlinearities of the detection, the Carré is more sensitive than the calibrated-shift algorithms (except the three-frame algorithm). It seemed to us that, despite the longer expression to calculate $\phi(u, v)$, the Carré algorithm is more appropriate because it takes into account the true shift that occurs at each point of the imaged object if the calibration of the phase-shifter device is not desired. Note that the phase shifts $\Delta\phi_k(u, v)$ can be calculated *a posteriori* by a formula given in Refs. 2 and 18. Numerical simulations showed us that a phase shift near 2.1 rad leads to minimal error of the calculated phase $\phi(u, v)$, probably because the fourth interferogram is redundant to the first. It is then recommended to approach this value. Before implementing this algorithm, we calibrated the detection system (gray levels versus the incident intensity) in order to correct the interferograms from the nonlinearities that are present (mainly owing to the frame grabber) before calculating $\phi(u, v)$.

3. Experiment

A. Setup

As is shown in Subsection 3.B, the problem of the optimization of the setup is not obvious, and one has to be able to vary easily the parameters such as the total intensity of the writing beam and the ratio between their intensities. The angle between them is fixed because it shows a maximum in the diffusion regime generally at ~60°.

Also, because different types of objects with different reflectivities are expected to be tested with our setup, we chose to develop a setup as versatile as possible in terms of the intensities of the object and the reference beams. Therefore the laser beam, provided by an argon laser (Spectra-Physics 2060) emitting up to 2.2 W at 514 nm, is separated into object and reference beams by means of a variable beam splitter (VBS) (Fig. 3). In the reference arm, the beam is collimated in order to cover the crystal input face, while in the object arm, the beam is allowed to diverge in order to illuminate large objects. Shutters (SH1 and SH2) are placed in both arms to provide the holographic recording–reading sequence. The phase shifting is introduced by translation of a plane mirror in the path of the reference beam by means of a piezoelectric translator (PSPZT).

The holographic head consists of the combination of a first dichroic polarizer (P1), a photorefractive crystal (C), a second polarizer (P2), and a CCD camera with an imaging objective. The crystal is BSO supplied by Sumitomo with a 1 cm × 1 cm input face and 3 mm of thickness. The first polarizer has its transmission axis such that the polarizations of the diffracted and the transmitted beams at the crystal output are crossed. The camera, with an objective of 26-mm focal length opened at 1.1, is set as close as possible to the crystal to obtain a maximum field of view of roughly 20 cm × 30 cm at a distance of ~1 m. The typical available intensities from white diffuse objects are found to be 8 $\mu W/cm^2$ at the level of the crystal (after P1). The angular configuration is such that the measured deformations are quasi out of plane.

The video signal is digitized with an 8-bit-resolution frame grabber for the subsequent analysis of interferograms. The time delay between successive acquisitions is 1 s, taking into account the control of both the piezoelectric phase shifter and frame acquisition (768 × 512 pixels).

B. Optimization of the Setup

In order to design a HI based on PRC's, one has to set different parameters in order to optimize the recording and the reading properties of the crystal (diffraction efficiency and scattered noise). Also, great atten-

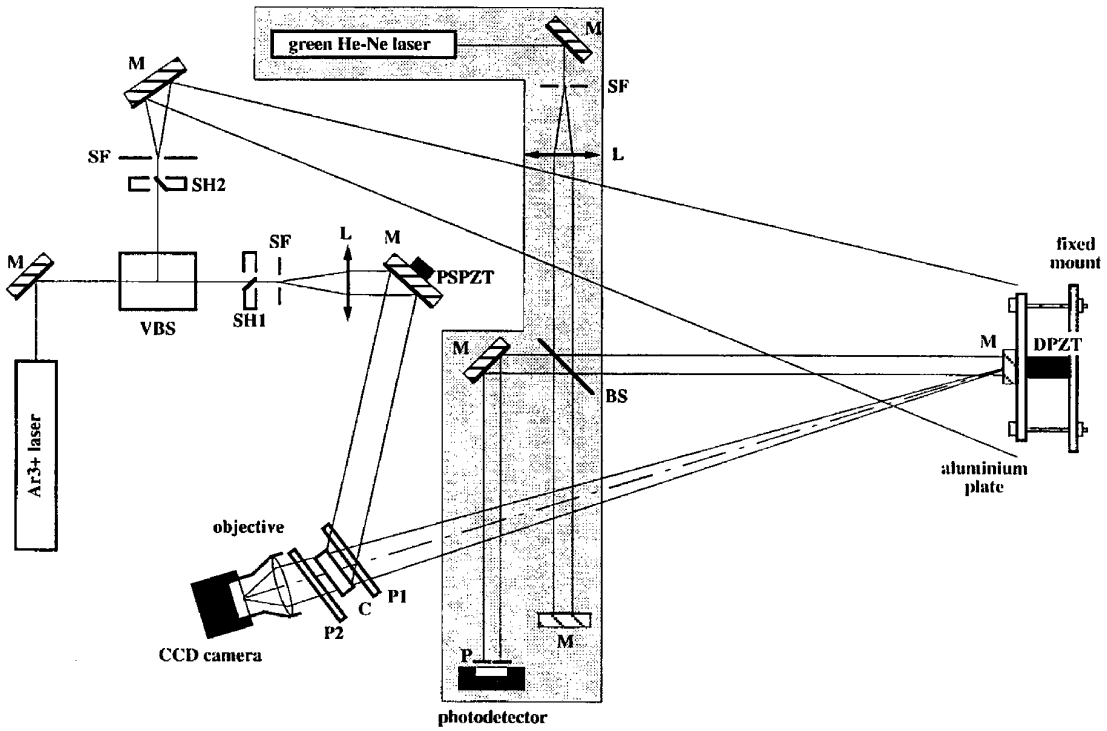

Fig. 3. Holographic interferometer setup that uses a BSO crystal. DPZT, deformation piezoelectric translator.

tion is paid to the characteristic time of the first hologram erasure because it is of importance in the phase-shifting sequence at the reading process; in other words, we try to have a time sufficiently long to acquire the four frames with fringe contrast not too rapidly varying between images. We study in Subsection 3.C the effect of contrast decrease on the error on the calculated phase.

Various authors have already studied parameters that can optimize HI with sillenite crystals, particularly BSO's. The diffraction efficiency in the diffusion regime has a maximum for writing angles of 55° (for our crystal) and has a ratio R between reference and object intensities equal to one.[10] Because we work with diffusively reflecting objects, the intensity of light reaching the crystal is generally low. To increase it, one can set the crystal closer to the object, but this is unsatisfactory because it reduces the possible observed area. The objects are then located at a certain distance from the holographic head, depending on the size to be observed. Low object intensity then means equally low reference intensity (because ideally $R = 1$) and therefore weak total intensity. Because the characteristic recording/erasure times are inversely proportional to incident intensity,[5] this leads to a long erasure time and is satisfactory for phase shifting. On the other hand, low reference intensity implies a very low diffracted intensity because generally η does not exceed a fraction of percent. So the difficulty in observing an interferogram is high even with the polarization balance at the output of the crystal. The solution is to increase the reference intensity ($R > 1$). Moreover, this situation is interesting in order to optimize the ratio between the amount of residual unpolarized light coming from the object and the diffracted light, as shown by Troth and Dainty.[10] This noise of polarization, which cannot be stopped by the second polarizer, is mainly caused by the diffusion and the stress birefringence in the crystal. They disturb the process of intensity equalization between the interfering beams. In our setup we found an optimal value of $R = 30$ at the level of the crystal.

For HI connected with phase-shifting phase measurement, the erasure of the diffracted beam (and thus of the interferogram) has to be as slow as possible. This means that a rather low intensity level of the readout beam has to be considered, which reduces the diffracted signal and requires the use of a sensitive CCD camera. In our case we used a Sony ICX027 CCD with a sensitivity of 0.3 lux at $f/1.2$.

C. Error Analysis

Basically there are two types of errors: systematic and random errors. The first category includes the miscalibration (linear and nonlinear) of the phase-shifter device, the nonlinearities of the detection system (CCD camera and/or frame grabber), and the quantization (resolution limit) of the measured intensity that is actually sampled on 8 bits. Additionally, as explained in Subsection 2.A, in the particular case of a PRC-based holographic interferometer, the modulation decrease between successively acquired interferograms has to be taken into account. The effect of these error sources on the calculated phase $\phi(u, v)$ can be computed provided that some experimental parameters are determined first.

The second category includes air turbulences and vibrations, which are considered to be more important than the systematic errors. For quantitative evaluation with temporal phase shifting, in which the acquisition of interferograms is delayed, the modulation $m(u, v)$ of the successively acquired interferograms should remain as constant as possible.

The modulation of the interferogram is classically defined by

$$m = \frac{I_{\max} - I_{\min}}{I_{\max} + I_{\min}} = \frac{2(I_d I_t)^{1/2}}{I_d + I_t}, \tag{7}$$

where $I_{\max}$ and $I_{\min}$ are the maximum and the minimum intensities observed in the interferogram, I_t is the transmitted (direct) object intensity after P2 and remains constant, and I_d is the diffracted intensity after P2 and exponentially decreases with respect to time:

$$I_d = I_d(t) = I_{d,0} \exp(-t/\tau). \tag{8}$$

In Eq. (8), $I_{d,0}$ is the diffracted intensity at the first instant when the interferogram is observed, and τ is the characteristic time of the erasure. Ideally, one could set the transmission axis of polarizer P2 such that $I_{d,0} = I_t$. The modulation is then given by

$$m = m(t) = \frac{2 \exp(-t/2\tau)}{1 + \exp(-t/\tau)}. \tag{9}$$

Figure 4 shows the plots of the temporal behavior of the modulation as a function of t/τ compared with the exponential decrease of the diffracted intensity.

One can now simulate the error of the phase calculated, $\phi(u, v)$, caused by variation of modulation for a known distribution of phase $\phi_i(u, v)$. For this, $m(u, v)$ in Eq. (4) has to be replaced by $m_k(u, v)$ and calculated with Eq. (9) at the different instants of image acquisition t_k. The corresponding interferograms I_k are obtained by injection of the quantities $I_0(u, v)$, $m_k(u, v)$, $\phi_i(u, v)$ and $\Delta\phi_k(u, v)$. The mean intensity $I_0(u, v)$ is set at the value 127.5, which is half the complete dynamic of an image, sampled on 8 bits, in term of gray levels. Note that this is an ideal case because we assume that the complete dynamic is used for the observation of the interferogram. Without loss of generality, the initial phase function $\phi_i(u, v)$ can be taken as a plane function of pixel coordinates. In the case of the Carré algorithm, the phase shift $\Delta\phi_k(u, v)$ is taken as 2.1 rad for all (u, v), a value recommended in Subsection 2.B.

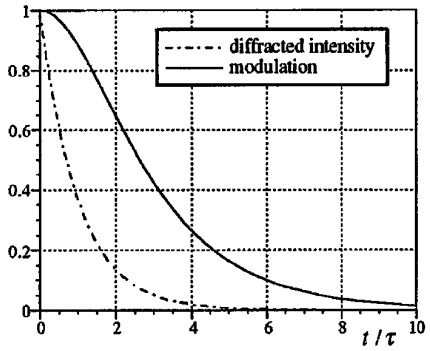

Fig. 4. Plot of the modulation m as a function of t/τ compared with the diffracted-intensity exponential decrease.

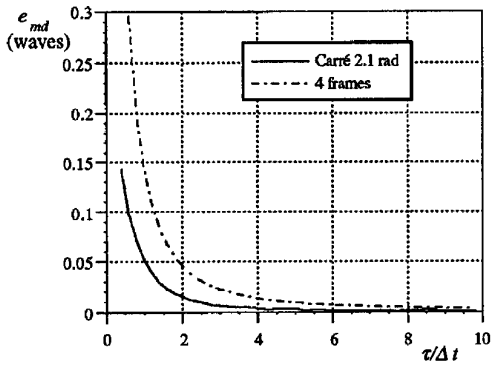

Fig. 5. Computed rms error (as a fraction of a wave) made on the calculated phase in the presence of a modulation decrease.

Once the four interferograms are formed, the phase $\phi(u, v)$ is recalculated with an expression such as Eq. (5) or (6) by following the algorithm considered. The phase error that is due to a modulation decrease for a point with coordinates (u, v) is $e_{\mathrm{md}}(u, v) = \phi(u, v) - \phi_i(u, v)$. Because e_{md} depends on coordinates, we have to consider the peak-to-valley or the rms value as an expression of the error on the phase calculation in the presence of a modulation decrease. In Fig. 5 we present the rms error calculated as a function of $\tau/\Delta t$, where τ is the erasure time and Δt is the phase-step delay for two algorithms (Carré and four-frame). The curves of Fig. 5 show an rms error smaller for the Carré algorithm than for the four-frame algorithm. For a $\tau/\Delta t$ of 5, e_{md} reaches $\lambda/300$ for the Carré algorithm and $\lambda/100$ for the four-frame algorithm. For smaller $\tau/\Delta t$, the error increases rapidly.

Figure 6 presents results of measurement of the erasure time τ for the typical object-beam intensity available in our setup (8 $\mu W/cm^2$) and different values of R (or, equivalently, of the readout intensity). It shows that for the optimum value of $R = 30$ the

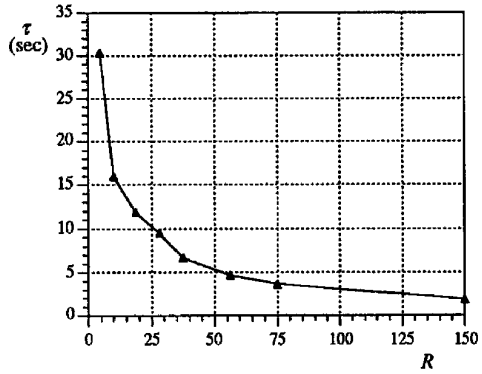

Fig. 6. Erasure time in seconds measured as a function of the intensity ratio R for an object-beam intensity of 8 $\mu W/cm^2$.

erasure time is found to be ~10 s. The acquisition time interval of our setup is 1 s, so the error on the calculated phase is $\lambda/1000$ rms.

The other systematic errors can be computed easily with the same procedure as for the modulation-decrease error.

The linear miscalibration of the phase shifter is obviously inconsequential in the case of the Carré algorithm. Nonlinear miscalibration is also possible, but the calibration sheet of the piezoelectric translator reports a variation of 0.08% from the linearity. Therefore the error on the phase can be considered as negligible if one refers to the graphs of Creath.[2,18]

The possible nonlinearity of the detection system was measured and found to come from the frame grabber. The measured intensities (given in gray levels) were then corrected. The error after this correction was computed and found to be less than $e_{\mathrm{nld}} = \lambda/1000$ rms.

The quantization of the measured intensities was also computed. This error depends on both the resolution limit in the number of gray levels (here from 0 to 255) and the fringe modulation. For the ideal case, in which the complete detection dynamic is used and the modulation is one, this error is found to be $e_{\mathrm{q}} = \lambda/3000$ rms. In practice we generally do not use the whole dynamic, and, owing to the detector noise, the lowest detected level is not zero. For the different measurement examples presented below, we observed fringes with a mean level of 50 and a modulation of 0.8. In this case, the computed error is roughly $e_{\mathrm{q}} = \lambda/1000$ rms.

The random error sources in our setup were minimized. For eliminating air turbulence, a Plexiglass-top table around the setup was satisfactory; for reducing the vibrations, the experiment was set on a pneumatically compensated optical bench. Despite all these precautions, a small amount of disturbances remained that could cause error in the measured phase. In order to have an idea of this error, we performed the interferometric measurement of a tilt between two plane mirrors and deduced the phase difference $\phi_t(u, v)$ by the phase-shifting technique after correction from the detection nonlinearity. The phase profile was then fitted by a plane function $\phi_{\mathrm{fit}}(u, v)$, and the rms error e_{vib} was calculated by means of the differences $\phi_t(u, v) - \phi_{\mathrm{fit}}(u, v)$. e_{vib} was found to be roughly $\lambda/40$, which showed that the vibration was the most significant error source.

The total error e_ϕ on the measured phase is calculated by summing the squares of all the errors calculated or measured that are mentioned above:

$$e_\phi = [(e_{\mathrm{md}})^2 + (e_{\mathrm{nld}})^2 + (e_{\mathrm{q}})^2 + (e_{\mathrm{vib}})^2]^{1/2} \approx e_{\mathrm{vib}} = \lambda/40. \tag{10}$$

This figure is considered as the error in the subsequent measurements.

D. Certification Experiment

This experiment consists of measuring the deformation of an aluminum plate by phase shifting. The plate is a square of 13 cm × 13 cm and is attached at its corners to a fixed mount and placed at ~1 m from the crystal. The static deformation is applied at the rear side with a piezoelectric translator (DPZT). The deformation is independently measured with a Michelson interferometer (drawn inside the gray area frame of Fig. 3). For this, a small mirror is glued at the center of the plate front side and serves as a mobile mirror in this second interferometer. The laser is a green He–Ne laser (λ = 543.5 nm), and the Michelson interference fringe intensity is measured through a pinhole (P) with a photodetector. A displacement of the plate shifts these fringes, and the modulated photodetector signal is plotted by a chart recorder.

Figure 7 summarizes the sequence of operations. First, both shutters are opened, and the hologram of the underformed plate is recorded. Second, at time t_a, both shutters are shut down. Between t_a and t_b, the piezoelectric actuator at the rear side of the plate induces an elongation of value L to the center of the plate. Meanwhile, the shifts of the fringes in the

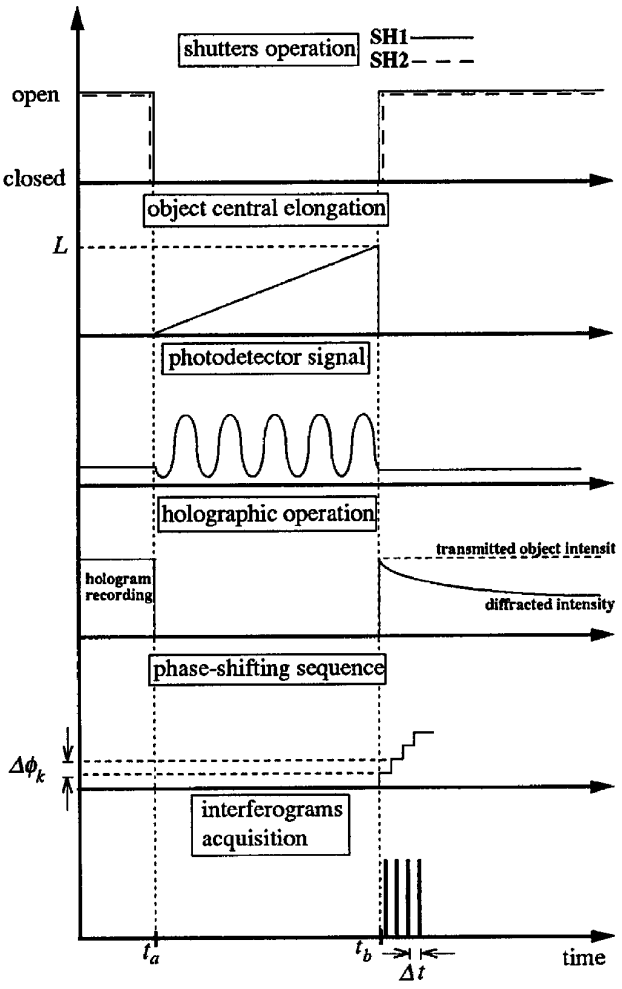

Fig. 7. Certification experiment: sequence of operations.

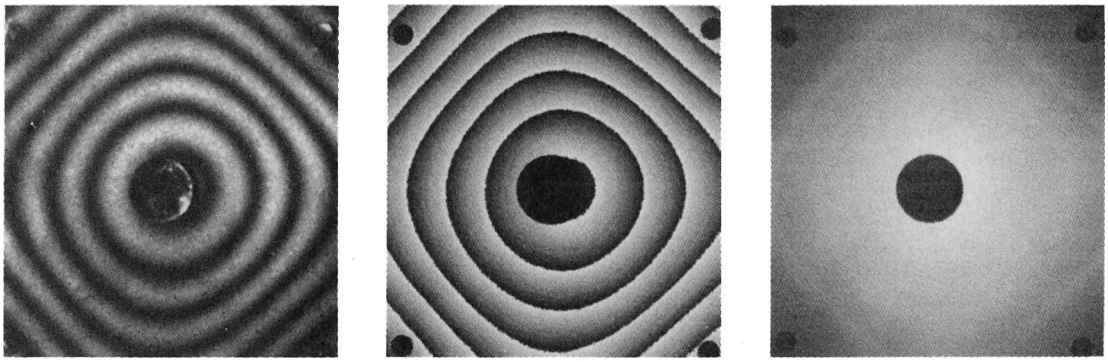

Fig. 8. Certification experiment: (a) one of the interferograms obtained after deformation of the plate (the zones corresponding to the central mirror and the attachment points are masked), (b) the corresponding phase calculated modulo 2π by phase shifting, (c) the phase map after unwrapping of (b).

Michelson interferometer are recorded. Third, at time t_b, the elongation is stopped, and both shutters are opened. At t_b, the phase-shifting sequence is started in the holographic interferometer, and four interferograms are successively acquired. Therefore the phase difference between the undeformed and the deformed plates is calculated by use of these interferograms [Fig. 8(a)] in Eq. (6). After this, the modulo 2π phase image [Fig. 8(b)] is unwrapped, and the continuous phase map [Fig. 8(c)] corresponding to the plate deformation is obtained. Note that the glued mirror masks the center of the plate, and the phase difference cannot be calculated directly at these points. The corresponding phase difference is estimated by interpolation with a polynomial function. Figure 9 shows phase values taken along a line that passes through two opposite attached points and the polynomial fit. The offset in phase is adjusted so as to have the zero point at the level of the attachment points. Assuming that these points are not moved during the elongation, the phase difference ϕ_c between the central point and one of them is calculated,

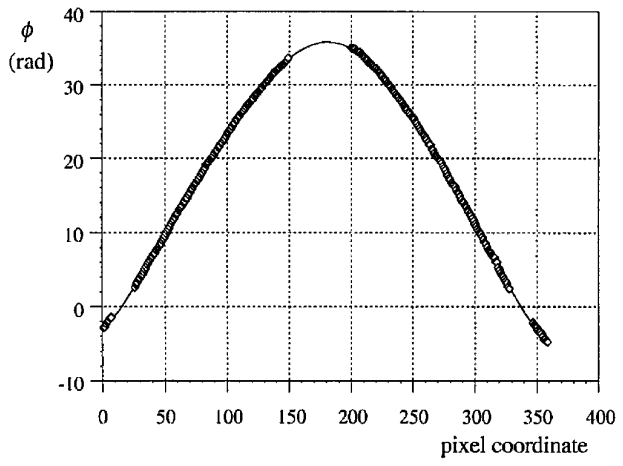

Fig. 9. Phase profile along the line passing through the lower-left and the upper-right attachment points. The solid curve represents the polynomial fit of the data to obtain the phase in the masked area.

and the central elongation L is given by

$$L = \frac{\phi_c \lambda}{2\pi[\cos(\theta_1) + \cos(\theta_2)]}, \tag{11}$$

where θ_1 and θ_2 are the angles between the normal to the object and the illumination and the observation directions, respectively.

The experiment was carried out four times for a given elongation of the piezoelectric transducer (DPZT). Table 1 gives the values of L measured by a Michelson interferometer and by holographic interferometry. The average of the four values measured by both methods is also given with a respective spread of measurement. This spread is found to be $\sim$10 nm for both methods and is smaller than the measurement error that is estimated for our holographic interferometer at $\lambda/40$, i.e., $\sim$13 nm at 514 nm.

4. Application

The setup was developed for monitoring displacements and deformations of diffusively reflecting surfaces. An interesting application is the detection of defects inside structures. The basic methodology of real-time HI for defect detection is the following. A hologram is recorded when the object is at the rest. Afterwards, the object is stimulated, and the interferogram shows fringes of the deformation undergone by the object under stimulation. The defect is visible, located in the fringe pattern, where a local differential deformation occurs owing to a different behavior of the defect under the stimulation. Additionally, a

Table 1. Results of Elongation Obtained by Holographic Interferometry and by a Michelson Interferometer

	Elongation L (nm)	
Experiment	HI	Michelson
1	1536	1549
2	1558	1569
3	1552	1547
4	1539	1558
Average	1546 ± 10	1555 ± 10

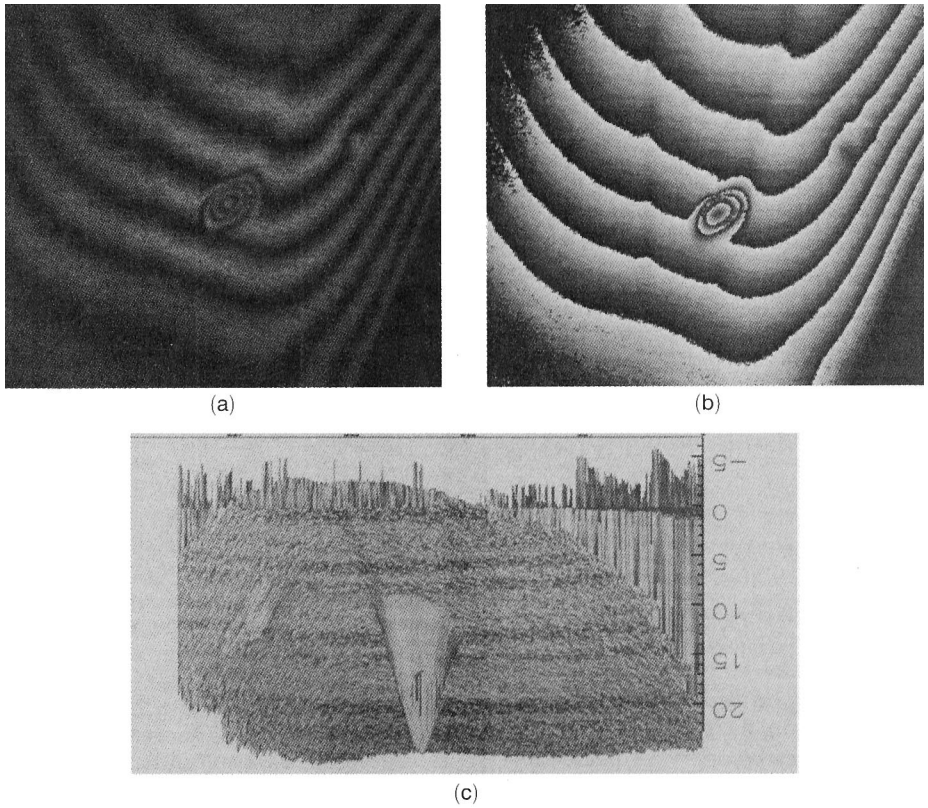

Fig. 10. Application to defects detection: (a) one of the interferograms obtained after thermal infrared stimulation of the composite sample, (b) the corresponding phase calculated modulo 2π by phase shifting, and (c) a three-dimensional view of the global deformation including defects (ordinates in radians).

phase-measurement technique, such as the phase-shifting described above, can be used to give a map of the complete deformation.

It is well known in nondestructive testing that the stimulation has to be adapted to the type of defect and structure. It is sometimes difficult to achieve the most suited stimulation all at once. So the experiment has to be carried out at different times with different types and magnitudes of stimulation. For this reason a photorefractive holographic interferometer is well suited because, once the interferogram is observed and processed, it disappears, and after a few seconds, the instrument is ready for a new measurement.

In the nondestructive experiment presented below, the object is a composite structure containing parts with different thicknesses in which manufacturing defects are located beneath the external skin and consequently are not visible. Because the object has a black, weakly reflecting surface, it is coated with white powder, which allows diffusive reflection.

The object is placed 1.1 m from the crystal, the object intensity is 9 $\mu W/cm^2$, and the intensity ratio R is set at 30. The observed area measures 20 cm $\times$ 30 cm. The stimulation is thermal heating provided by two 500-W infrared lamps placed at the rear side of the sample (typically 0.5 s). Once the stimulation is stopped, the hologram is not read directly because the sample is rapidly varying in shape owing to the thermal relaxation. After a few seconds, the time at which the sample is found relaxed, the shutters are opened, and an interferogram is observed sufficiently stable to permit the phase-shifting process. Figure 10(a) shows one of the four interferograms of the phase-shifting sequence, Fig. 10(b) shows the phase image calculated modulo 2π, and Fig. 10(c) a shows a three-dimensional plot of the sample deformation (in phase values) after phase unwrapping. One clearly observes two defects and two lines that correspond to a difference in thickness of the composite structure.

5. Conclusion

In this paper we have presented a real-time holographic interferometer with a BSO crystal used in the diffusion regime. The diffusion regime enables one to use the anisotropic self-diffraction technique, which is of interest for its polarization separation properties between diffracted and transmitted object beams. This technique was already used by different authors, but it was not yet connected to a phase-measurement technique such as phase shifting, permitting quantitative evaluation of the interferogram. Our interferometer is designed to monitor quantitative deformations of large diffusively reflecting objects. For this, the holographic head (containing successively a polarizer, a BSO crystal, a second polarizer, an imaging objective, and a CCD camera) is placed at a distance from the object such that a large area can be covered.

The intensity in the object beam is then low (typically from 8 to 10 $\mu W/cm^2$) at the level of the crystal, but the modulation of the fringes in the interferogram can be maximized by proper polarization balance of diffracted and transmitted object beams. The weak intensities are an advantage for the phase-shifting evaluation because the interferogram is observed for a time sufficiently long to not cause significant error in the calculated phase. On the other hand, these weak luminous levels appear as a lowest practical limit. For a decrease in this level, e.g., for increasing observation areas, larger crystals and special light-collecting systems have to be investigated. We conducted a certification experiment of the deformation of a plate, which was measured also with another method for comparison. Results by both methods were found in extremely good accordance. An interesting application is the observation of defects in structures that can be observed by local differential deformation under stimulation.

This work is supported by the General Direction of Technologies and Research at the Ministery of Walloon Region of Belgium. We thank Dominique Derauw at the Centre Spatial de Liège for his efficient phase-unwrapping algorithm developed during synthetic aperture radar interferometry project SSTC-TELSAT-III (contract T3/12/012).

References

1. C. M. Vest, *Holographic Interferometry* (Wiley, New York, 1979).
2. P. K. Rastogi, ed., *Holographic interferometry: Principles and Methods*, Vol. 68 of Springer Series in Optical Sciences (Springer-Verlag, Berlin, 1994).
3. P. Smigielski, *Holographie Industrielle* (Teknea, Toulouse, 1994).
4. P. Hariharan, *Optical Holography: Principles, Techniques and Applications*, Vol. 2 of Cambridge Studies in Modern Optics (Cambridge U. Press, Cambridge, UK, 1986).
5. P. Günter and J.-P. Huignard, eds., *Photorefractive Materials and Their Applications: Survey of Applications*, Vol. 62 of Topics in Applied Physics (Springer-Verlag, Berlin, 1989).
6. M. P. Petrov, S. I. Stepanov, and A. V. Khomenko, *Photorefractive Crystals in Coherent Optical Systems*, Vol. 59 of Springer Series in Optical Sciences (Springer-Verlag, Berlin, 1991).
7. S. I. Stepanov, "Applications of photorefractive crystals," Rep. Prog. Phys. **57,** 39–116 (1994).
8. P. Günter and J.-P. Huignard, eds., *Photorefractive Materials and Their Applications: Fundamental Phenomena*, Vol. 61 of Topics in Applied Physics (Springer-Verlag, Berlin, 1988).
9. H. J. Tiziani, "Real-time metrology with BSO crystals," Opt. Acta **29,** 463–470 (1982).
10. R. C. Troth and J. C. Dainty, "Holographic interferometry using anisotropic self-diffraction in $Bi_{12}SiO_{20}$," Opt. Lett. **16,** 53–55 (1991).
11. V. I. Vlad, D. Popa, M. P. Petrov, and A. A. Kamshilin, "Optical testing by dynamic holographic interferometry with photorefractive crystals and computer image processing," in *Optical Testing and Metrology III: Recent Advances in Industrial Optical Inspection*, C. Grover, ed., Proc. Soc. Photo-Opt. Instrum. Eng. **1332,** 237–244 (1990).
12. D. Dirksen and G. von Bally, "Holographic double-exposure interferometry in near real time with photorefractive crystals," J. Opt. Soc. Am. B **11,** 1858–1863 (1994).
13. H. J. Tiziani, "Fringe analysis in holography with BSO applications," in *Second French-German Congress on Applications of Holography*, P. Smigielski, ed. (HOLO3, Saint-Louis, France, 1988).
14. A. A. Kamshilin and M. P. Petrov, "Continuous reconstruction of holographic interferograms through anisotropic diffraction in photorefractive crystals," Opt. Commun. **53,** 23–26 (1985).
15. H. Kogelnik, "Coupled-wave theory of thick hologram gratings," Bell Syst. Tech. J. **48,** 2909–2947 (1969).
16. S. Mallick, D. Rouède, and A. G. Apostolidis, "Efficiency and polarization characteristics of photorefractive diffraction in a $Bi_{12}SiO_{20}$ crystal," J. Opt. Soc. Am. B **4,** 1247–1259 (1987).
17. A. Marrakchi, R. V. Johnson, and A. R. Tanguay, Jr., "Polarization properties of photorefractive diffraction in electro-optic and optically active sillenite crystals (Bragg regime)," J. Opt. Soc. Am. B **3,** 321–336 (1986).
18. D. W. Robinson and G. T. Reid, eds., *Interferogram Analysis: Digital Fringe Pattern Measurement Techniques* (Institute of Physics, London, 1993).
19. T. M. Kreis, "Review of digital processing of holographic interferograms," in *Third French-German Congress on Applications of Holography*, P. Smigielski, ed. (HOLO3, Saint-Louis, France, 1991).